Submitted to ApJL. Draft version dated June 21, 2016.
Preprint typeset using LaTeX style emulateapj v. 05/12/14

FRONTIER FIELDS CLUSTERS: ORIGIN OF THE X-RAY-BRIGHT GAS IN THE LARGE-SCALE FILAMENT CROSSING MACS J0717.5+3745

G. A. Ogrean[1, †], C. Jones[2], N. Werner[1], T. Whalen[3], R. J. van Weeren[2, ‡], W. Forman[2]

[1]KIPAC, Stanford University, 452 Lomita Mall, Stanford, CA 94305, USA; gogrean@stanford.edu
[2]Harvard-Smithsonian Center for Astrophysics, 60 Garden Street, Cambridge, MA 02138, USA; and
[3]University of Maryland, College Park, MD 20742, USA;
Submitted to ApJL. Draft version dated June 21, 2016.

ABSTRACT

We present results from deep *Chandra* observations of the large-scale filament extending SE from the Frontier Fields cluster MACS J0717.5+3745. The gas within the filament is found to have a temperature of $1.58^{+0.51}_{-0.25}$ keV and a density of $\sim 10^{-4}$ cm^{-3}. The filament density corresponds to a high baryon over-density of ~ 250, which can be explained by the fact that we are probing only the densest part of the filament. The filament properties are consistent with numerical simulations and with the few other observational results reported to date. Within the filament, ~ 2 Mpc away from the cluster center, there is a galaxy group with a mass of $\sim 5 \times 10^{13}$ M$_\odot$ and a temperature of ~ 3 keV. This group is likely infalling for the first time towards the cluster. NW of the cluster, ~ 670 kpc from the center, there is a ram pressure-stripped core that appears to have traversed the densest parts of the cluster after entering the ICM from the direction of the filament. This core is probably a later stage of the galaxy group seen in the filament. We detect a density discontinuity N-NE of the core, which we speculate is associated with a cold front. We do not detect a temperature jump across the density discontinuity. The non-detection is likely caused by a combination of poor count statistics and multiple superimposed substructures.

Keywords: Galaxies: clusters: individual: MACS J0717.5+3745 — Galaxies: clusters: intracluster medium — X-rays: galaxies: clusters

1. INTRODUCTION

In the ΛCDM cosmological model, structure in the Universe is organized in a filamentary web in which large-scale cosmic filaments connect virialized massive structures such as clusters and groups of galaxies (e.g., Einasto et al. 1994). Approximately a third of the total bayonic matter is expected from hydrodynamic simulations to be contained in these large-scale filaments (e.g. Davé et al. 2001), in the form of low-density gas with temperatures of $10^5 - 10^7$ K. One of the main signatures of cosmic filaments is soft X-ray emission. However, the low density of the gas within the filaments poses a significant observational challenge, which causes detections to strongly depend on fortuitous alignments of the filaments with our line of sight. As a consequence, there have been only a handful of filament detections, among which the one in MACS J0717.5+3745 (Ebeling et al. 2004), the one between A222-A223 (Dietrich et al. 2005; Werner et al. 2008), and several in A2744 (Eckert et al. 2015).

Clusters of galaxies grow via the infall of gas and less massive structures along cosmic filaments (e.g., Springel et al. 2006). During infall and subsequent collision with the cluster, less massive structures will be ram-pressure stripped as they fly through the cluster's denser regions. Consequently, depending on their original density, these structures are either fully destroyed, or their compact cores survive and develop tails in their wake. An example of the latter scenario is seen in the cluster 1E 0657–558 (Elvis et al. 1992), in which the collision of a massive cluster with a cluster about 1/10 of its mass (Springel & Farrar 2007; Mastropietro & Burkert 2008) resulted in the famous "bullet" morphology of the less massive structure (Markevitch et al. 2002).

Here, we present results from *Chandra* observations of the merging galaxy cluster MACS J0717.5+3745. MACS J0717.5+3745 ($z = 0.546$; Ebeling et al. 2001, 2007) is one of the most complex merging systems discovered to date, being the site of collisions between four substructures (Ma et al. 2009; Medezinski et al. 2013). The superposition of the dark matter halos of these substructures also makes MACS J0717.5+3745 the largest known gravitational lens (Zitrin et al. 2009; Medezinski et al. 2013). The analysis of shallower *Chandra* observations of the cluster by Ma et al. (2009) found hot regions with temperatures ~ 20 keV, remnant cool cores with temperatures of ~ 5 keV, and density and temperature jumps at the interface between the cluster and the SE filament. The authors speculated that the jumps are caused accretion of gas from the filament onto the cluster. More recently, we have analyzed the thermodynamical properties of the ICM of MACS J0717.5+3745 using deeper *Chandra* observations (van Weeren et al., submitted). In this letter, we present the physical properties of the SE filament connected to MACS J0717.5+3745, and those of the substructures along the filament.

In Section 2, we summarize the processing of the *Chandra* datasets. The properties of the filament are discussed in Section 3, while those of the substructures in the filament are discussed in Section 4. The properties of the

† Hubble Fellow
‡ Clay Fellow

NW core that flew through the cluster are presented in Section **??**. Our conclusions are summarized in Section 5.

Throughout the paper we assume a ΛCDM cosmology with $H_0 = 70$ km s^{-1} Mpc^{-1}, $\Omega_m = 0.3$, and $\Omega_\Lambda = 0.7$. For these parameters, 1 arcmin at the redshift of MACS J0717.5+3745 ($z = 0.546$) corresponds to a linear distance of approximately 383 kpc.

2. DATA PROCESSING AND BACKGROUND MODELING

Chandra observed MACS J0717.5+3745 four times between Jan 2001 and Dec 2013, for a total of 243 ks. Of the four ObsIDs, two (1655 and 16235) were taken in FAINT mode, while the other two (4200 and 16305) were taken in VFAINT mode. More details about the observation parameters can be found at the Chandra Data Archive.

The ObsIDs were reprocessed to apply the newest calibration files as of Jan 2004. Time periods affected by soft protons were removed from the data using the CIAO script *deflare*. ObsID 1655 had residual soft proton flares and we decided to remove it from the spectral analysis. The total clean exposure time after flare filtering was approximately 209 ks (193 ks ignoring ObsID 1655). Point sources were detected in the energy bands $0.5 - 2$ and $2 - 7$ keV using the script *wavdetect*, were visually confirmed, and excluded from the analysis. The instrumental background was subtracted using the stowed background files available in CalDB 4.6.3. Before subtraction, the instrumental background files were normalized to have the same $10 - 12$ keV count rate as the corresponding source files.

The sky background was modeled as the sum of unabsorbed emission from the Local Hot Bubble, absorbed emission from the Galactic Halo, and absorbed emission from unresolved X-ray sources. The hydrogen column density was fixed to 8.36×10^{20} cm^{-2}, corresponding to the sum of the atomic and molecular hydrogen column densities in the direction of MACS J0717.5+3745[4] (Kalberla et al. 2005; Willingale et al. 2013). All the foreground components were assumed to have solar metallicities equal to those reported by Feldman (1992).

A more detailed description of the data processing and the background modeling is provided by van Weeren et al., submitted. Our analysis can also be reproduced by the reader by downloading the datasets from the Chandra Data Archive and running the JUPYTER notebook[5] available at `https://github.com/gogrean`.

3. X-RAY EMISSION FROM THE FILAMENT

To define the region of the filament that is least contaminated by ICM emission, we examined the surface brightness profile in a rectangular region aligned with the filament. In this region, the surface brightness decreases away from the cluster center, and then increases again when the region intersects the SE group located along the filament; there is no radial range in this region where the surface brightness is flat. This suggests that the ICM of MACS J0717.5+3745 contaminates the filament, and this contamination needs to be considered when modeling the filament emission.

To model the filament and the contamination from the ICM, we extracted spectra in two rectangular regions: one centered on the filament, and one positioned to the SW of it; NE of the filament, the signal-to-noise is too low for any meaningful information to be extracted from the spectrum. These regions are shown in Figure 1. The regions were chosen to avoid the bright parts of the ICM, as well as emission from the SE galaxy group. The emission in the SW region was modeled with a single thermal component, while the emission in the filament region was modeled with two thermal components–one describing ICM contamination, whose parameters were linked to those of the thermal component used to describe the SW region, and one describing emission from the filament. The spectra from the two regions were fitted simultaneously. Table 1 lists the best-fitting parameters obtained for a gas metallicity of 0.2 solar. Varying the metallicity causes only minor changes to the best-fitting parameters, well within the statistical uncertainty ranges. In the JUPYTER notebook supporting this letter, we also list the results obtained for metallicities of 0 and 0.1 solar.

Table 1
Parameters of the regions used for the spectral analysis. The regions are shown in Figure 1. Uncertainties are quoted at the $\Delta C = 1$ level.

FOREGROUND AND BACKGROUND

Model Component	Temperature[a]	Normalization[b]
Local Hot Bubble	$0.135^{+0.007}_{-0.008}$	$7.21^{+0.30}_{-0.18} \times 10^{-7}$
Galactic Halo	$0.59^{+0.09}_{-0.08}$	$2.78^{+0.45}_{-0.44} \times 10^{-7}$
Unresolved Background Sources ObsID 16235/16305	–	$4.44^{+0.35}_{-0.37} \times 10^{-7}$
Unresolved Background Sources ObsID 4200	–	$7.02^{+0.49}_{-0.58} \times 10^{-7}$

LARGE-SCALE FILAMENT

Model Component	Temperature[a]	Normalization[b]
On Filament	$1.58^{+0.51}_{-0.25}$	$4.00^{+0.56}_{-0.60} \times 10^{-5}$
Off Filament	$11.55^{+9.09}_{-3.95}$	$1.55^{+0.14}_{-0.10} \times 10^{-5}$

GROUP IN THE FILAMENT

	Temperature[a]	Normalization[b]
	$3.87^{+0.66}_{-0.51}$	$(1.77 \pm 0.13) \times 10^{-4}$

FLY-THROUGH CORE

Model Component	Temperature[a]	Normalization[b]
Core	$6.82^{+1.88}_{-1.36}$	$3.41^{+0.29}_{-0.25} \times 10^{-4}$
N+S of Core	$7.47^{+1.11}_{-0.86}$	$2.08^{+0.77}_{-0.78} \times 10^{-4}$
Ahead of Core	$5.06^{+1.61}_{-0.98}$	$8.52^{+0.88}_{-0.77} \times 10^{-5}$
Behind Core	$10.89^{+2.05}_{-1.27}$	$3.92^{+0.10}_{-0.09} \times 10^{-4}$

[a] Units of keV.
[b] Units of cm^{-5} arcmin^{-2} for the thermal components, and photons keV^{-1} cm^{-2} s^{-1} arcmin^{-2} at 1 keV for the power-law components.

The XSPEC normalizations of the thermal components listed in Table 1 are defined as:

$$\mathcal{N} = \frac{n_e \, n_H \, V}{10^{14} \, \pi \, S_{reg} \, D_A^2 \, (1+z)^2} \, , \qquad (1)$$

if we assume the density to be constant in each region, where n_e is the electron number density, n_H is the hydrogen number density, V is the volume of the region, S_{reg} is the projected area of the region, D_A is the angular size distance to the cluster, and z is the cluster redshift.

To calculate the density of the filament in the region

[4] http://www.swift.ac.uk/analysis/nhtot/index.php
[5] Running the notebook requires the bash_kernel package.

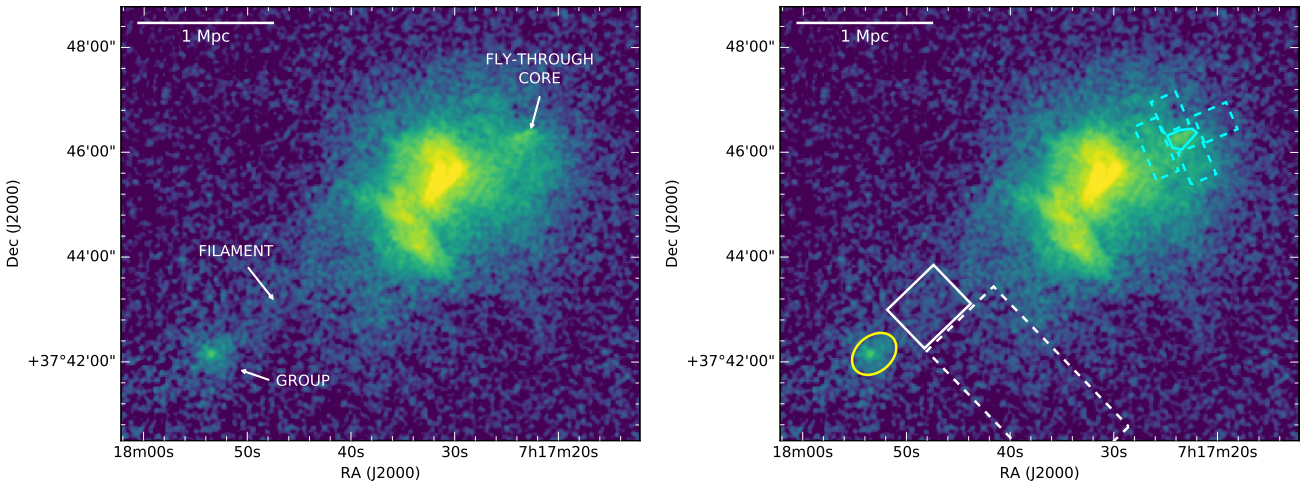

Figure 1. *Left:* Chandra 0.5 – 4 keV surface brightness map of MACS J0717.5+3745, showing the features discussed in this work. The image was exposure- and vignetting-corrected. Point sources were subtracted and the gaps were filled by sampling the regions surrounding the point sources. The gaps were filled to create a more visually appealing figure. However, the imaging analysis was done on images that did not have the gaps filled. The images used in the analysis are available online as supporting material. *Right:* Regions used in the spectral analysis. The regions of main interest are drawn in solid lines, while the regions used to characterize the contaminating/surrounding emission are drawn in dashed lines. The best-fitting parameters obtained for the gas in these regions are listed in Table 1.

shown in Figure 1, we assumed that in 3D the region is a parallelepiped with four rectangular faces: two perpendicular to the line of sight, and two parallel to it. Jauzac et al. (2012), citing Ebeling et al., in prep., quoted a filament inclination angle $\theta \sim 75$ degrees with respect to the plane of the sky. They also determined the filament has a diameter $D_{\rm fil} \sim 3$ Mpc at the radius from which our spectra were extracted and a length of ~ 19 Mpc. Therefore, the volume of the parallelepiped corresponding to our region is:

$$V \equiv V_{\rm ppp} = S_{\rm reg} D_{\rm fil} / \cos\theta \,, \qquad (2)$$

The projected region has a length of 1.2 arcmin ($\approx$ 460 kpc) and a width of 1 arcmin ($\sim$ 380 kpc), therefore $S_{\rm reg} = 1.2$ arcmin^2. Assuming $n_{\rm e} = 1.2\, n_{\rm H}$ (e.g., Böhringer & Werner 2010), and finally substituting Eq. 2 in Eq. 1, the electron number density in the X-ray bright part of the filament is $\sim 2 \times 10^{-4}$ cm^{-3}. The critical density of the Universe at the redshift of MACS J0717.5+3745 is 1.7×10^{-29} g cm^{-3}. Assuming the total baryon density is 4.4% the critical density of the Universe (Kirkman et al. 2003), the filament is overdense by a factor of ~ 450 compared to the mean baryon density of the Universe. Assuming a baryon mass fraction of 0.15 (e.g., Mantz et al. 2014), the mass density of the filament is $\sim 3 \times 10^{13}$ M$_\odot$ Mpc^{-3}. The filament density is therefore in excellent agreement with the density calculated from the weak lensing data by Jauzac et al. (2012) for the same filament geometry. The filament density corresponds to an overdensity of $\sim 100 - 150$ relative to the critical density of the Universe.[6]

For the densities calculated above, the mass of the filament in the region from which the spectra were extracted is $\sim 6 \times 10^{13}$ M$_\odot$, with $\sim 9 \times 10^{12}$ M$_\odot$ in baryons.

The calculations made above can be found in the supporting JUPYTER notebook accompanying this paper.

[6] Jauzac et al. (2012) calculate an overdensity of $206 \pm 46\ \rho_{\rm crit}$, about 65% higher than our value, but this appears to be a miscalculation; our filament mass density values are consistent.

4. GROUP IN THE FILAMENT

The group of galaxies within the large-scale filament is located a little over 2 Mpc SE of the cluster center, chosen to be at RA = 07 : 17 : 30.025, Dec = +37 : 45 : 18.58 for consistency with Jauzac et al. (2012). The small size of the group and its large distance from the cluster implies that it is falling for the first time towards MACS J0717.5+3745, rather than having traversed the cluster from the NW to the SE.

We measured the temperature and the brightness of the group by extracting spectra from an elliptical region shown in Figure 1. We assumed a group metallicity of 0.2 solar. The best-fitting parameters are summarized in Table 1. The normalization is equivalent to a luminosity of $(1.05 \pm 0.09) \times 10^{43}$ erg s^{-1} in the energy band 0.1 – 2.4 keV. Based on the luminosity-mass scaling relations for galaxy groups (e.g., Connor et al. 2014), the group's luminosity corresponds to a mass of $\sim 5 \times 10^{13}$ M$_\odot$.

In Figure **??**, we show the *Chandra* surface brightness profiles of the group in four sectors chosen such that two are aligned with the filament, while the other two are perpendicular to the filament axis.

5. SUMMARY

MACS J0717.5+3745 ($z = 0.546$) is a massive galaxy cluster selected as one of the six Frontier Fields targets. The cluster is the most morphologically complex merger, being the site of collisions between at least four subclusters. SE of the cluster, there is a large-scale cosmic filament that was first reported by Ebeling et al. (2004). Some of the subclusters involved in the merger have likely traveled along this filament before colliding with the previously existing structure. Jauzac et al. (2012) determined from optical data that the filament is ~ 19 Mpc long and ~ 1.6 Mpc wide. Part of the filament that is near the cluster is also visible at X-ray wavelengths. So far, the thermodynamic properties of large-scale filaments have only been studied in a handful of merging clusters (Werner et al. 2008; Eckert et al. 2015; Bulbul et al. 2016). Here, we used deep *Chandra* observations

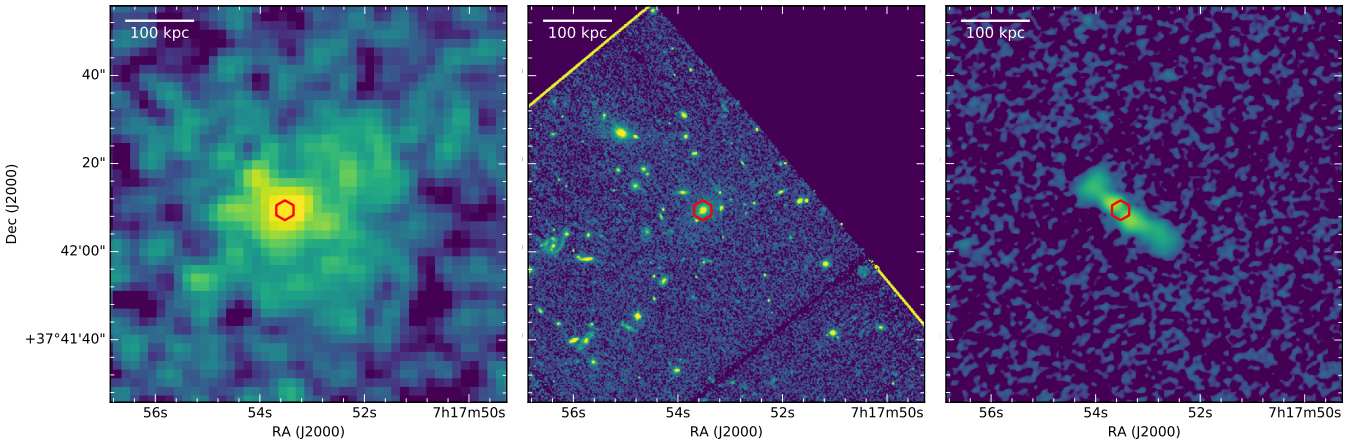

Figure 2. *Chandra* (left), *HST* (middle), and *VLA* (right) images of the region occupied by the galaxy group in the filament. The red hexagon marks the position of the group's BCG. The position of the BCG coincides with those of the radio AGN and of the X-ray peak.

of MACS J0717.5+3745 to study the properties of the large-scale filament extending SE of the cluster center, and those of the substructures along the filament. Below is a summary of our results:

- The filament has a temperature of $1.58^{+0.51}_{-0.25}$ keV and a density of $\sim 10^{-4}$ cm^{-3}. These are consistent at the 90% confidence level with the properties of the other filaments studied in X-ray (Werner et al. 2008; Eckert et al. 2015; Bulbul et al. 2016).
- The filament is over-dense by a factor of $\sim$ 300 compared to the mean baryon density of the Universe.
- The total mass contained in the X-ray-bright region of the filament is $\sim 2 \times 10^{13}$ M$_\odot$. Approximating the transversal density profile of the filament with the model presented by Gheller et al. (2015), the mass of the whole filament (i.e. considering its full length of 19 Mpc) is $(1-2) \times 10^{14}$ M$_\odot$.
- A little over 2 Mpc SE of the cluster center, embedded within the filament, there is a galaxy group with a temperature of $\sim$ 3 keV and an X-ray luminosity of $\sim 10^{43}$ erg s^{-1} in the energy band 0.1−2.4 keV. The mass of the group is estimated to be $\sim 5 \times 10^{13}$ M$_\odot$. This group is likely approaching the cluster for the first time.

GAO acknowledges support by NASA through a Hubble Fellowship grant HST-HF2-51345.001-A awarded by the Space Telescope Science Institute, which is operated by the Association of Universities for Research in Astronomy, Incorporated, under NASA contract NAS5-26555. R.J.W. is supported by a Clay Fellowship awarded by the Harvard-Smithsonian Center for Astrophysics.

This research made use of APLPY, an open-source plotting package for PYTHON hosted at `http://aplpy.github.com`, and of ASTROPY, a community-developed core PYTHON package for Astronomy (Astropy Collaboration et al. 2013). This research has also made use of NASA's Astrophysics Data System, and of the cosmology calculator developed by N. Wright (Wright 2006). The surface brightness modeling used PYXEL, a PYTHON open-source modeling package for X-ray astronomy.

The optical data shown in the paper is based on observations made with the NASA/ESA Hubble Space Telescope, and obtained from the Hubble Legacy Archive, which is a collaboration between the Space Telescope Science Institute (STScI/NASA), the Space Telescope European Coordinating Facility (ST-ECF/ESA) and the Canadian Astronomy Data Centre (CADC/NRC/CSA).

REFERENCES

Astropy Collaboration, Robitaille, T. P., Tollerud, E. J., et al. 2013, A&A, 558, A33
Böhringer, H., & Werner, N. 2010, A&A Rev., 18, 127
Bulbul, E., Randall, S. W., Bayliss, M., et al. 2016, ApJ, 818, 131
Connor, T., Donahue, M., Sun, M., et al. 2014, ApJ, 794, 48
Davé, R., Cen, R., Ostriker, J. P., et al. 2001, ApJ, 552, 473
Dietrich, J. P., Schneider, P., Clowe, D., Romano-Díaz, E., & Kerp, J. 2005, A&A, 440, 453
Ebeling, H., Barrett, E., & Donovan, D. 2004, ApJ, 609, L49
Ebeling, H., Barrett, E., Donovan, D., et al. 2007, ApJ, 661, L33
Ebeling, H., Edge, A. C., & Henry, J. P. 2001, ApJ, 553, 668
Eckert, D., Jauzac, M., Shan, H., et al. 2015, Nature, 528, 105
Einasto, M., Einasto, J., Tago, E., Dalton, G. B., & Andernach, H. 1994, MNRAS, 269, 301
Elvis, M., Plummer, D., Schachter, J., & Fabbiano, G. 1992, ApJS, 80, 257
Feldman, U. 1992, Phys. Scr, 46, 202
Gheller, C., Vazza, F., Favre, J., & Brüggen, M. 2015, MNRAS, 453, 1164
Jauzac, M., Jullo, E., Kneib, J.-P., et al. 2012, MNRAS, 426, 3369
Kalberla, P. M. W., Burton, W. B., Hartmann, D., et al. 2005, A&A, 440, 775
Kirkman, D., Tytler, D., Suzuki, N., O'Meara, J. M., & Lubin, D. 2003, ApJS, 149, 1
Ma, C.-J., Ebeling, H., & Barrett, E. 2009, ApJ, 693, L56
Mantz, A. B., Allen, S. W., Morris, R. G., et al. 2014, MNRAS, 440, 2077
Markevitch, M., Gonzalez, A. H., David, L., et al. 2002, ApJ, 567, L27
Mastropietro, C., & Burkert, A. 2008, MNRAS, 389, 967
Medezinski, E., Umetsu, K., Nonino, M., et al. 2013, ApJ, 777, 43
Springel, V., & Farrar, G. R. 2007, MNRAS, 380, 911
Springel, V., Frenk, C. S., & White, S. D. M. 2006, Nature, 440, 1137
Werner, N., Finoguenov, A., Kaastra, J. S., et al. 2008, A&A, 482, L29
Willingale, R., Starling, R. L. C., Beardmore, A. P., Tanvir, N. R., & O'Brien, P. T. 2013, MNRAS, 431, 394
Wright, E. L. 2006, PASP, 118, 1711
Zitrin, A., Broadhurst, T., Rephaeli, Y., & Sadeh, S. 2009, ApJ, 707, L102